

L-arginine as Corrosion and Scale Inhibitor of Steel in Synthetic Reservoir Water

K. F. Khaled^{1,2,*}, N. S. Abdel-Shafi^{2,3}, N. A. Al-Mubarak⁴, M. S. Alonazi⁴

¹ Materials and Corrosion Laboratory, Chemistry Department, Faculty of Science ,Taif University, Taif, Hawiya 888, Kingdom of Saudi Arabia

² Electrochemistry Research Laboratory, Chemistry Department, Faculty of Education, Ain Shams University, Roxy, Cairo, Egypt

³ Chemistry Department, Faculty of Science ,Hail University, Hail, Kingdom of Saudi Arabia

⁴ Chemistry Department, Faculty of Science ,Princess Norah University, Al-Ryadh, Kingdom of Saudi Arabia

*E-mail: khaledrice2003@yahoo.com

Received: 26 November 2015 / Accepted: 14 December 2015 / Published: 1 February 2016

Effect of L-arginine as corrosion and calcium carbonate scale inhibitor has been evaluated using scale inhibition efficiency experiments, electrochemical measurements (Electrochemical impedance spectroscopy, EIS, potentiodynamic polarization and linear polarization measurements) and Monte Carlo simulation measurements. The evaluation shows that L- Arginine may be considered as a multifunctional inhibitor. Scale inhibition efficiency experiments as well as electrochemical experiments confirm that the scale /inhibition action of L-arginine in synthetic reservoir water. Results of electrochemical experiments shows that, under the selected experimental conditions L-arginine presents sufficient inhibition for steel corrosion in synthetic reservoir water. Monte Carlo simulation used to find low energy adsorption sites found on L-arginine as well as Fe (111) surface as the temperature of the system is slowly decreased. The results indicated that L-arginine could relax on a iron surface by adsorption through the nitrogen/oxygen atoms with the lone pair of electrons in its molecule.

Keywords: Scale inhibition; Corrosion inhibition; EIS; DFT; Monte Carlo Simulations

1. INTRODUCTION

An influential research effort is found to replace chromate due to the toxic nature of chromate. Chromium (VI) compounds are extensively applied as corrosion inhibitors in aqueous media. Their high efficiency cost ratio has made chromates typical corrosion inhibitors[1-7]. However, due to their

oxidizing characters, chromate concentration in the medium must be checked periodically, to avoid undesirable corrosion results, since concentrations lower than a critical value can promote pitting corrosion[8-10]. Environmental rules are increasing the force to remove some of compounds widely used in industrialized applications to inhibit corrosion. Hexavalent chromium-based processes are one of the most affected by these regulations. Some green alternatives to chromates are currently rising, oriented mainly in minimizing environmental impact and, secondarily, in providing efficient corrosion inhibition [11, 12].

In view of the close relationship of the problems of scale to the corrosion of metals in open cooling systems, they will also be treated in the work. Attempts to minimize corrosion without considering other problems are generally unsuccessful, and corrosion inhibitors usually added as part of the package treatment for this system[13-16]. Because we are dealing with a circulating system, undesirable deposits are quite varied in nature and can come from many sources. Scales are classified as precipitated suspended solid, inorganic scaling, phosphate sludge, and metal deposits[17].

The most common scale is calcium carbonate[17-19]. In practice, these scales are present at the same time in a mixture, and the deposit is heavily interspersed with the corrosion products [17, 20]. Calcium carbonate precipitates because of the nature of the operation of the cooling-tower system. The makeup of water fed to the system generally has only a small amount of calcium in it and has little carbonate and some bicarbonate ions[17].

Environmentally green corrosion inhibitors are eco-friendly compounds that do not have any toxic heavy metals or any other toxic material. The success in using of those green naturally compounds to inhibit the corrosion of metals in aqueous environment have been reported by Khaled et al.[21, 22], Eddy et al.,[23-25] and Kamal et al.,[26-28].

This study seeks to add some insight into the steel corrosion in synthetic reservoir water in the absence and presence of L-arginine as possible antiscalent as well as corrosion inhibitor. L-arginine has been reported previously as corrosion inhibitor for copper metal in acidic medium[29] and is likely to be an efficient inhibitor for steel in synthetic reservoir water due to the presence of a different donor centers in its structure.

Also, molecule dynamics simulation method and density functional theory will be used to investigate the adsorption behavior of L-arginine at steel surface.

2. EXPERIMENTAL PROCEDURES

2.1. Scale inhibition tests

The experiments were carried out using a laboratory rig which represented a holder made of plexiglass where five similar glasses each with the capacity of 100 cm³ were placed. Scale forming solution is poured into the glasses, different amounts of the L-arginine being investigated were introduced and then they were covered with a common plexiglass lid. Then a thermocouple with stainless steel rings (samples) put on it was lowered into each glass through the holes in the lid. Scale

deposited on this rings when current was passed to the thermocouples. The studied solution was synthetic reservoir water, composed of salts in Table 1.

Table 1. Composition of synthetic reservoir water (made in distilled water).

COMPOUND	MOLARITY	GRAMS/LITER
CaCl ₂	0.81	119.07
MgCl ₂	0.09	8.69
NaCl	1.98	115.71
SrCl ₂	0.01	3.52
KCl	0.15	11.44
NaHCO ₃	0.00124	0.1042
BaCl ₂	0.0039	0.95

The composition was selected so, as during heating the solution, scale was deposited from it in the form of calcium carbonate. The total solution volume was 400 cm³. Each run lasted for 90 minutes. During this time the solution in the glasses was heated up to a temperature of 90 °C and was kept at this temperature for one hour. At the end of the run the thermocouples were removed from the glasses, the samples were rinsed with a small amount of distilled water, ethanol and were dried at a temperature of 80°C and then were weighted. The mass of the deposited on the samples scale was determined according to the change of their weight before and after the run. The degree of inhibition efficiency, *S*% for the scale formation process of the L-arginine addition with concentrations (10⁻⁶, 5 10⁻⁵, 10⁻⁴, 10⁻³ and 10⁻² M) was evaluated according to the equation:

$$S\% = \left(1 - \frac{Q}{Q_0}\right) \times 100 \quad (1)$$

where *Q*₀ scale mass deposited on the sample ,from the solution without introduction of L-arginine into it; *Q* scale mass deposited on the sample from the solution with L-arginin additive introduced into it, in grams.

2.2 Electrochemical corrosion inhibition tests

Electrochemical experiments were conducted using a conventional three-electrode electrolytic cell arrangement: saturated Ag/AgCl as a reference electrode, platinum gauze as a counter electrode, and the working electrode (*WE*) had the form of a cylindrical piece of steel. The counter electrode was separated from the working electrode by fritted glass. To minimize *IR* drop, the reference electrode was connected to a Luggin capillary. Solutions were prepared from synthetic reservoir water (Table 1), Prior to each experiment, the specimen was polished with a series of emery papers of different grit sizes up to 4/0 grit sizes, polished with Al₂O₃ (0.5 mm particle size). The working electrode washed several times with bidistilled water then with acetone and dried using a stream of air. The electrode potential allowed to stabilize for 60 minutes before starting the experiments. All experiments were carried out at 25 ± 1 °C.

Polarization resistance measurements were obtained by changing the electrode potential automatically from (-20 to 20 mV vs Ag/AgCl) at open circuit potential with scan rate of 2 mVs^{-1}

Potentiodynamic polarization curves were obtained by changing the electrode potential automatically from (-1.5 to 1.5 V vs Ag/AgCl) at open circuit potential with scan rate of 5.0 mVs^{-1} .

EIS measurements were carried out in a frequency range of 100 kHz to 40 mHz with amplitude of 5 mV peak-to-peak using ac signals at open circuit potential.

Measurements were performed with a Gamry Instrument Reference 3000 Potentiostat/Galvanostat/ZRA. This includes a Gamry framework system based on the ESA400, Gamry applications that include DC105 for dc corrosion measurements, EIS300 for electrochemical impedance spectroscopy measurements to calculate the corrosion current and the Tafel constants along with a computer for collecting the data. Echem Analyst 6.11 software was used for plotting, graphing and fitting data.

3. COMPUTATIONAL DETAILS

Computational details for this study was described elsewhere[30-35]. A brief summary for the computational techniques used in this study are described as follow:

Monte Carlo simulation techniques used to find the adsorption sites on both the steel surface and L-arginine molecules. L-arginine molecules, steel surface and solvent molecules had built using Materials studio 7.0, distributed by Accelrys, Inc. [36]. Condensed-phase optimized molecular potentials for atomistic simulation studies, COMPASS [37] is a classical force field used in optimizing the structures of the corrosion system.

Molecular mechanics (force field) tools are used to investigate the simulated corrosion system. The key approximation in these studies that the potential energy surface, on which the atomic nuclei move, is represented by a classical force field, which are developed by parameterising data from experiment and high level quantum mechanical calculations. COMPASS force field stands for, which is used to optimize the structures of all components of the corrosion system (iron substrate/solvent/inhibitor). The first step in this computational study is the preparation of a model of molecules, which will adsorb on the surface with optimized geometry (i.e. energy minimized). Among the different steps involved in the modeling approach is the construction of the iron surface from the pure crystal, the addition of the L-arginine molecule near to the surface, the definition of the potentials (i.e. the force field) to study the liquid–solid interaction, followed by the geometry optimization calculation.

4. RESULTS AND DISCUSSION

4.1 Scale inhibition test

The experimental results obtained are given in Fig. 1. Figure 1 shows the percent inhibition degree of scale formation in the form of calcium carbonate for different concentrations of L-arginine.

As the concentration of L-arginine increases the scale inhibition efficiency increases. It is generally agreed that the antiscalents operate by adsorption onto the mineral surface at growth sites, thereby preventing further crystal formation and deposition.

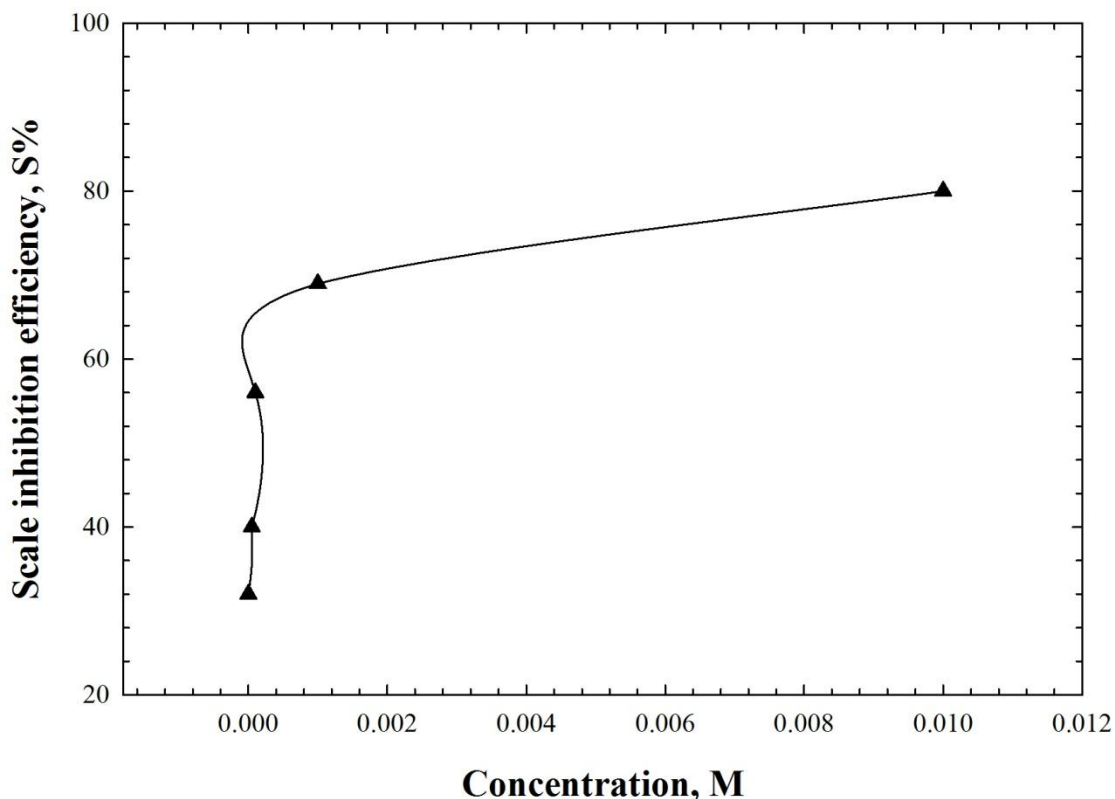


Figure 1. Percent inhibition of calcium carbonate scale by varying concentrations of L-arginine

4.2. Electrochemical investigations

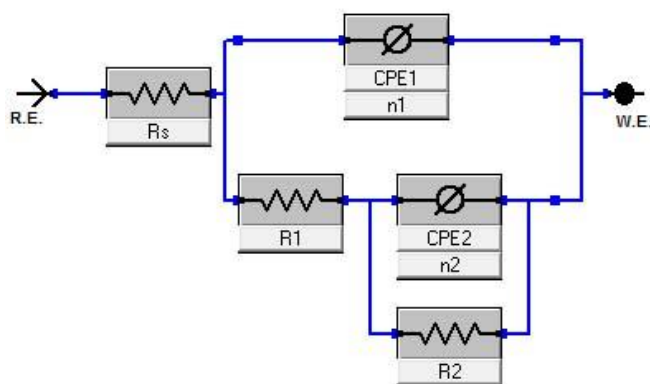


Figure 2. Equivalent circuit proposed to simulate the experimental impedance diagrams in the evaluation of API 5L X60 steel in the synthetic reservoir water in absence and presence of the studied compounds at 25 °C.

Equivalent circuit presented in Figures 2 is used to model the experimental EIS results depicted in Figures 3-5.

The results of the EIS measurements were depicted in Figures 3-5 as Nyquist and Bode plots. Figure 3 shows the EIS results for the steel electrode in absence of L-arginine molecules. Impedance measurements were conducted in synthetic reservoir water composed of several ions according to Table 1 without and with different concentrations of the studied L-arginine amino acid. Nyquist plots show depressed semicircles with its center under the real axis. This behaviour is distinguishing for solid electrodes and repeatedly referred to as frequency dispersion and explained due to the roughness and other inhomogeneities of the steel electrode [38-40]. The capacitive loop is attributed to the charge-transfer in the electrochemical corrosion [41]. The depression in the higher frequency loop is due to the surface inhomogeneity of structural or interfacial origin, such as those found in adsorption on solid electrodes [42].

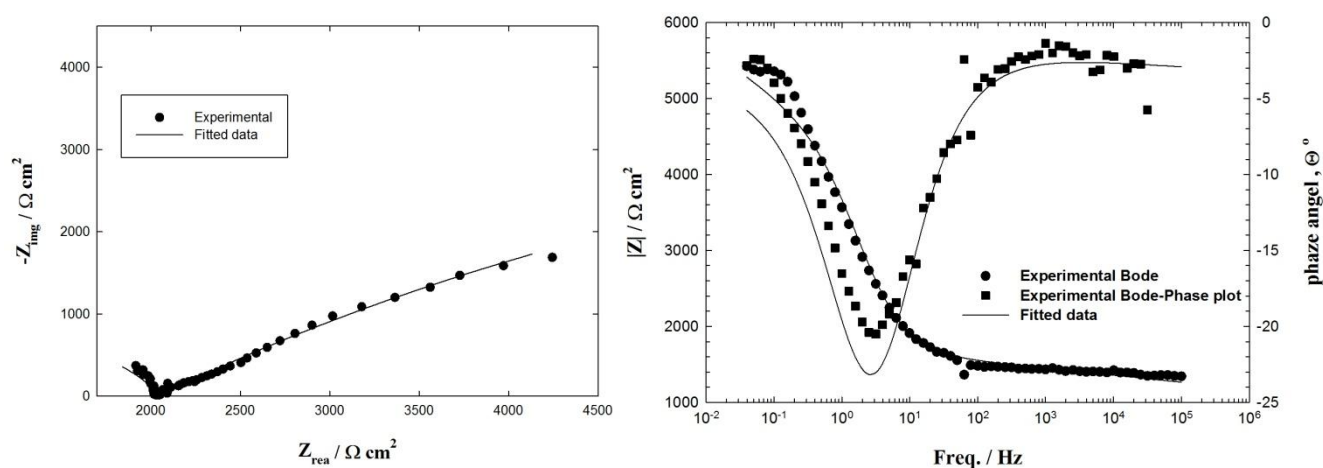


Figure 3. Nyquist and Bode plots for steel 5LX60 electrode in synthetic reservoir water at 25 ± 1 °C.

The interfacial impedance can be modeled in terms of a generalized equivalent circuit [43]. Curve fitting of the experimental results was performed with the program E-chem Analyst and confirmed using Zview impedance modeling software, in which the experimental data are fitting an equivalent circuit consisting of resistances R and the constant phase elements (CPEs). We substitute the classical capacitance C by the constant phase element (CPE) so that the phenomena related to the heterogeneous surface may be taken into account. The constant phase element is defined as: $CPE = [C(j\omega)^n]^{-1}$. The value of n of the CPE is about 0.7 to 0.9. The equivalent circuit that was found to reproduce most closely the impedance diagrams is shown in Figure 2. EIS plots presented in Figures 2-5 are modeled using an equivalent circuit presented in Figure 2, similar to the one proposed by several authors [44-46].

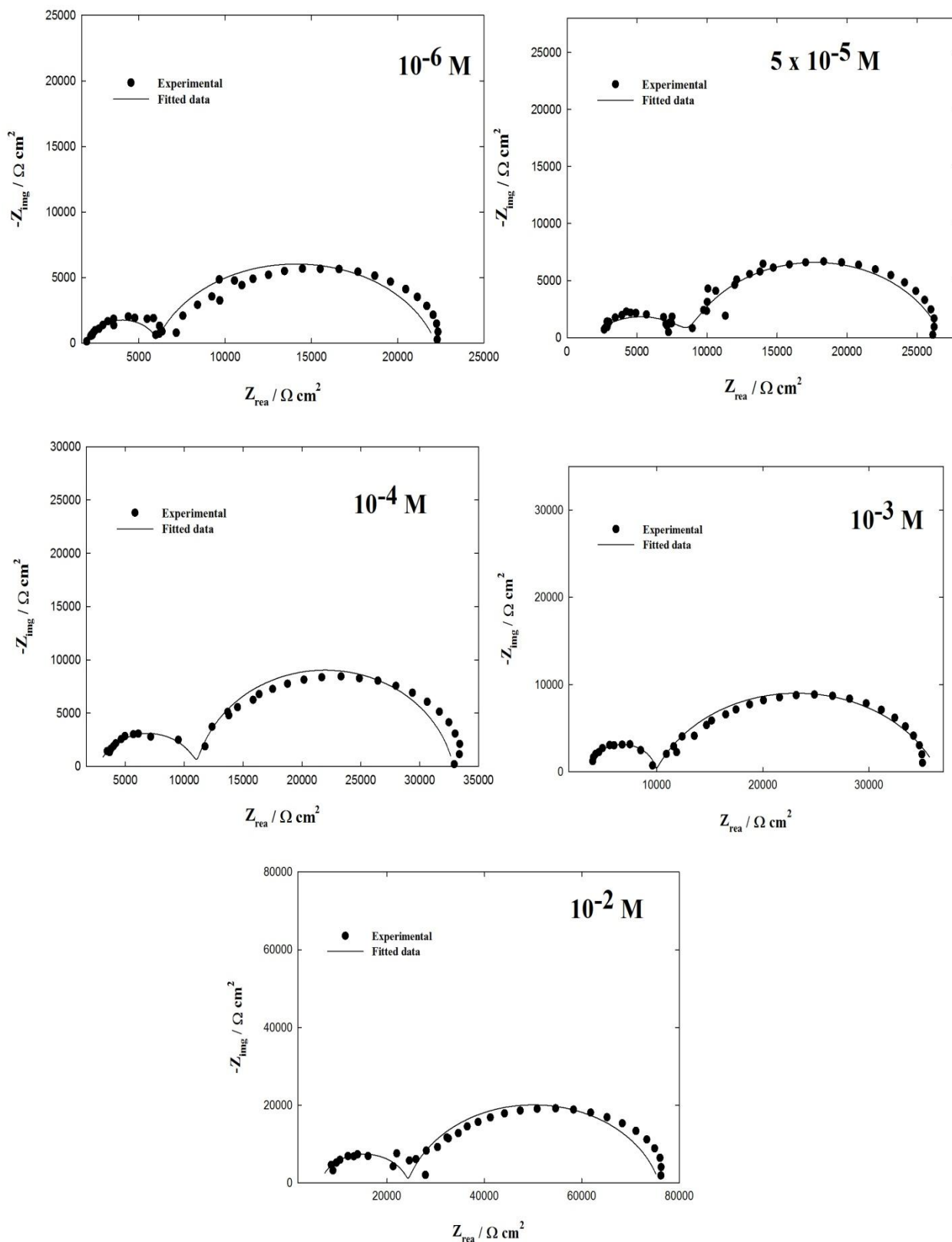


Figure 4. Nyquist plots for steel 5LX60 electrode in synthetic reservoir water in the presence of different concentrations of L-arginine at $25 \pm 1 \text{ }^\circ\text{C}$.

Table 2. Electrochemical parameters calculated from electrochemical impedance measurements on steel 5LX60 electrode in water without and with various concentrations of L-arginine at 25 ± 1 °C.

Conc. M	R_s $\Omega^{-1} \text{ cm}^2$	R_1 $\Omega^{-1} \cdot \text{cm}^2$	R_2 $\Omega^{-1} \cdot \text{cm}^2$	CPE_1 $\Omega^{-1} \text{cm}^{-2} \text{S}^n$	n_1	CPE_2 $\Omega^{-1} \text{cm}^{-2} \text{S}^n$	n_2	$R_1 + R_2$ $\Omega^{-1} \cdot \text{cm}^2$	E_{IMP} %
0	2.8	15240	2041	663.4e-6	0.523	2.677e-9	0.793	7047	0.00
10^{-6}	12.1	16170	4617.61	9.970e-6	0.815	16.73e-9	0.922	20787.61	66.1
$5 \cdot 10^{-5}$	16.34	17920	5807.27	10.69e-6	0.804	259.7e-9	0.594	23727.27	70.3
10^{-4}	27.26	21720	10754.65	7.292e-6	0.882	21.66e-9	0.805	32474.65	78.3
10^{-3}	35.34	26620	15326.43	7.756e-6	0.756	1.328e-9	0.911	41946.43	83.2
10^{-2}	63.1	51560	23408.09	3.041e-6	0.842	2.981e-9	0.875	74968.09	90.6

Electrochemical parameters obtained from the equivalent circuit presented in Figure 2 and inhibition efficiency is shown in Table 2. As the concentration of the L-arginine increases the values of polarization resistance increase and the constant phase element, CPE values are decreased. The constant phase element (CPE) with their n values where $1 > n > 0$ show double layer capacitors with some pores [47].

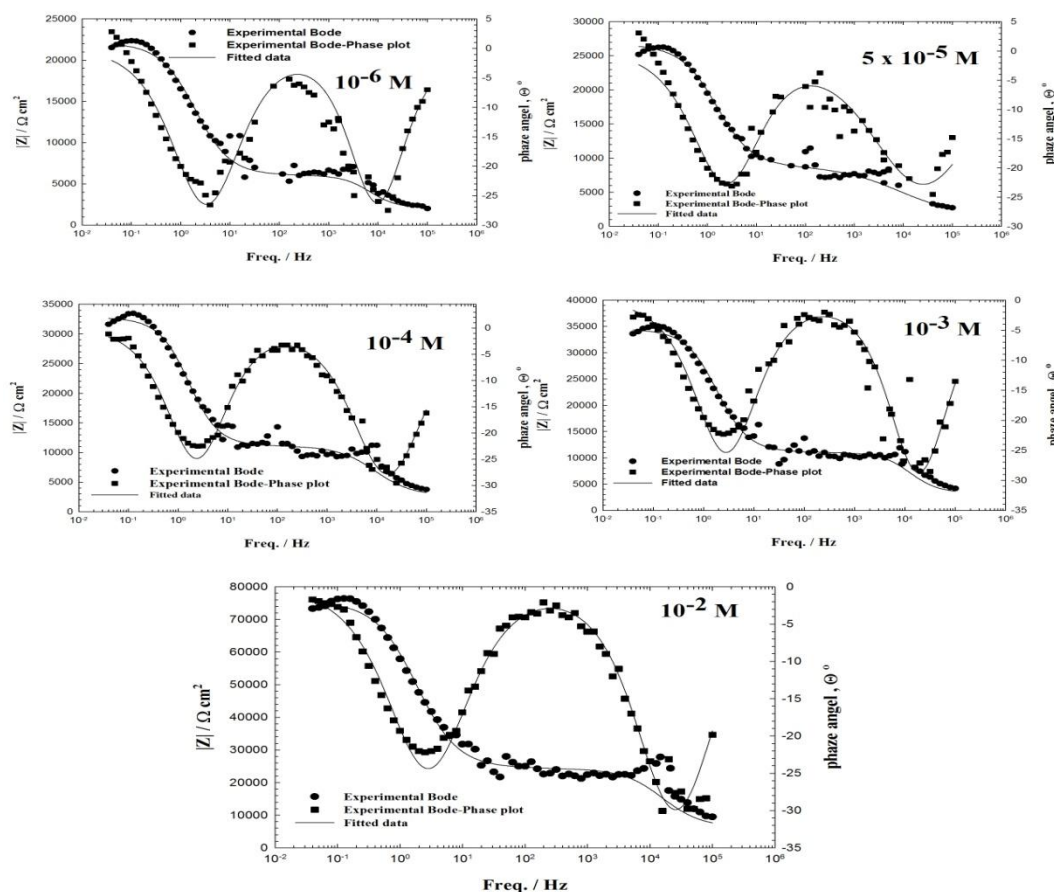


Figure 5. Bode plots for steel 5LX60 electrode in synthetic reservoir water in the presence of different concentrations of L-arginine at 25 ± 1 °C.

Adsorption of L-arginine on steel surface can be explained on the basis that , the decrease in constant phase element, CPE is a consequence of a decrease in local dielectric constant and/or an increase in the thickness of the double layer. The depressed semicircles in the Nyquist plots (Figures 3-5) are generally related with the relaxation of electrical double layer capacitors and the diameters of these depressed semicircles can be considered as the charge-transfer resistance ($R_{ct} = R_p$) [48].

Table 3. Electrochemical parameters calculated from polarization measurements on steel 5LX60 electrode in water without and with various concentrations of L-arginine at 25 ± 1 °C by potentiodynamic polarization measurements.

Conc. M	I_{corr} $\mu A.cm^{-2}$	$-E_{corr}$ mV	b_a $mV.dec^{-1}$	b_c $mV.dec^{-1}$	C.R mpy	E_T %
0.00	32.2	899	1282	607	14.70	----
10^{-6}	10.5	825	1432	1178	4.809	67.39
$5 \cdot 10^{-5}$	10.3	816	1345	1221	4.686	68.01
10^{-4}	8.52	809	1213	1225	3.892	73.54
10^{-3}	6.51	802	1152	1292	2.975	79.78
10^{-2}	3.6	799	1016	1254	1.643	88.81

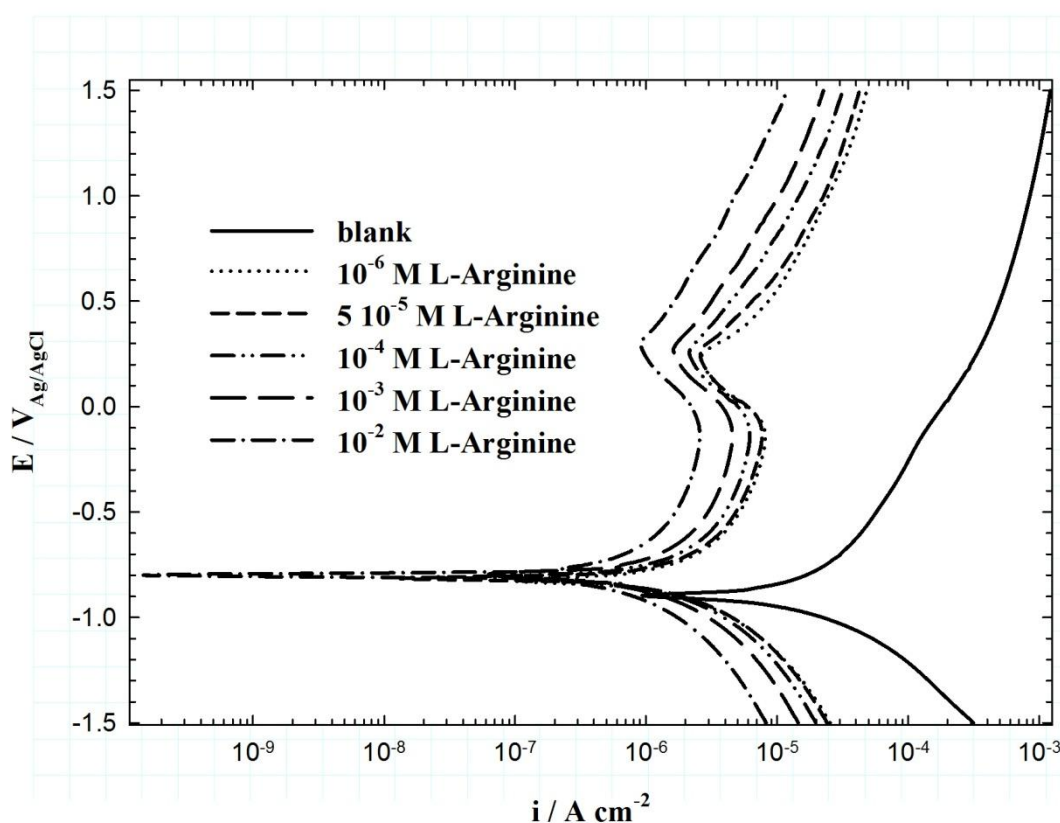


Figure 6. Anodic and cathodic polarization curves for steel 5LX60 electrode in synthetic reservoir water in without and with various concentrations of L-arginine at 25 ± 1 °C

Therefore, the inhibition efficiency, E_{IMP} % presented in Table 3 of the studied compound for the steel electrode can be calculated from the charge-transfer resistance as follows [44]:

$$E_{IMP} \% = \left(1 - \frac{R_p^o}{R_p}\right) \times 100 \quad (2)$$

where R_p^o and R_p are the polarization resistances calculated from EIS measurements for uninhibited and inhibited solutions ($R_p = R_1 + R_2$), respectively.

Addition of L-arginine reduces the cathodic and anodic currents, i_{corr} as illustrated in Figure 6. The corresponding electrochemical kinetics parameters such as corrosion potential (E_{corr}), anodic Tafel slopes (b_a), cathodic Tafel slopes (b_c) and corrosion current density (i_{corr}), obtained by extrapolation of the Tafel lines are presented in Table 3.

The inhibitor efficiency E_T % was evaluated from dc measurements using the following equation [42]:

$$E_T \% = \left(1 - \frac{i_{corr}}{i_{corr}^o}\right) \times 100 \quad (3)$$

where i_{corr}^o and i_{corr} correspond to uninhibited and inhibited current densities, respectively. E_T %.

Table 4. Electrochemical kinetic parameters and inhibition efficiencies recorded for Steel 5LX60 in synthetic reservoir water without and with various concentrations of L-arginine at 25 ± 1 °C calculated by polarization resistance measurements

Conc. M	Rp $\Omega.cm^2$	I_{corr} $\mu A.cm^{-2}$	$-E_{corr}$ mV _{Ag/AgCl}	C.R. mpy	E_{Rp} %
0.00	315.2	82.66	20.4	37.77	0.00
10^{-6}	816.6	31.91	20.53	14.58	61.39
$5 \cdot 10^{-5}$	917.0	28.41	20.41	12.98	65.63
10^{-4}	1.187e3	21.95	20.47	10.03	73.44
10^{-3}	1.456e3	17.89	20.38	8.174	78.35
10^{-2}	2.78e3	9.36	20.39	4.277	88.67

Table 4 shows the electrochemical kinetic parameters and inhibition efficiencies recorded for 5LX60 in synthetic reservoir water solutions without and with various concentrations of L-arginine at 25 ± 1 °C calculated by polarization resistance measurements. As can be seen from Table 4, the polarization resistances increase as the concentration increases, i.e. corrosion rate decreases and inhibition efficiency increases. The inhibition efficiency calculated from the following equation:

$$E_{R_p} \% = \left(1 - \frac{R_p^o}{R_p}\right) \times 100 \quad (4)$$

where R_p^o and R_p are the polarization resistances calculated from linear polarization resistance measurements for uninhibited and inhibited solutions, respectively.

4.3 Modeling Studies

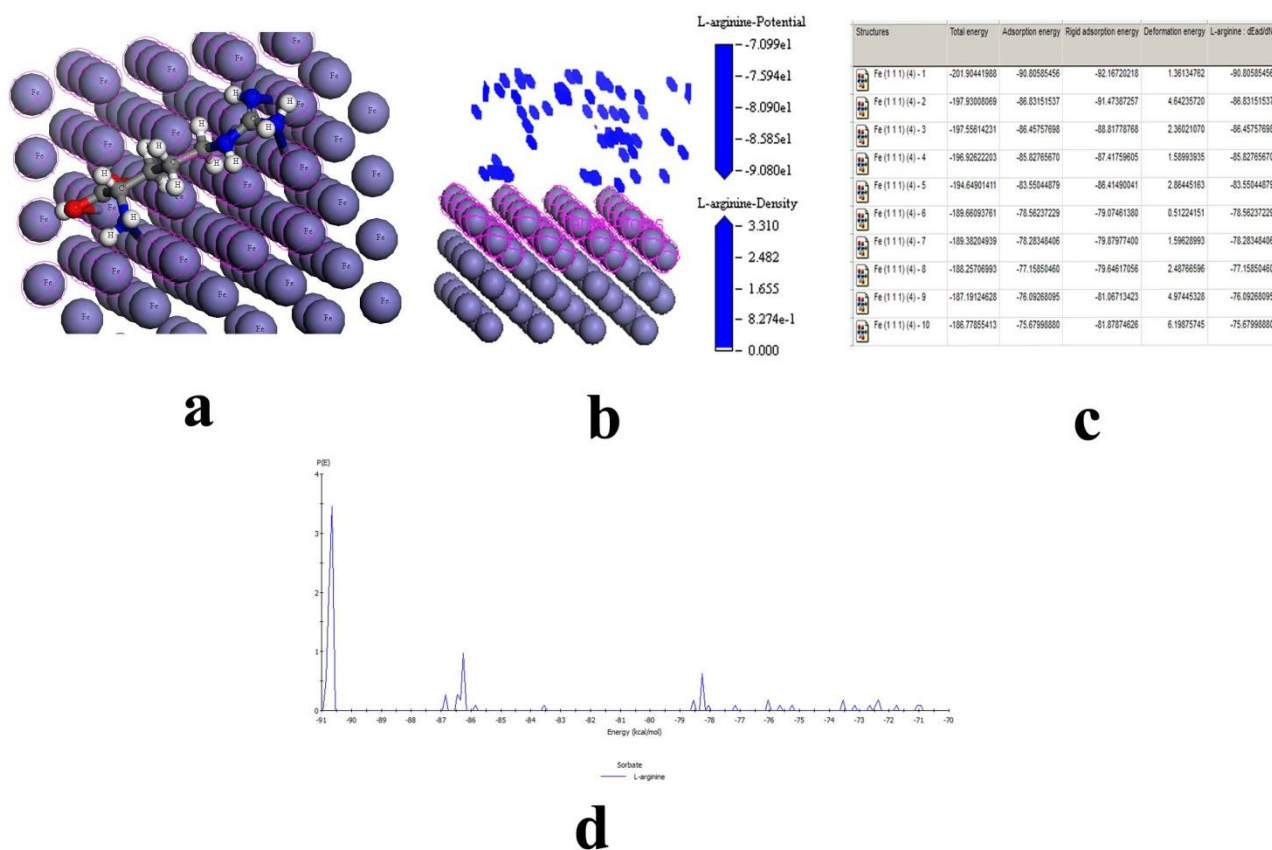


Figure 7. Computer simulation studies for adsorption of L-arginine on Steel surface: (a) Most stable configuration, (b) adsorption density , (c) output descriptors of the adsorption process, (d) adsorption energy curve.

This study is a continuation of our work on the corrosion inhibition of steel in acidic and neutral medium by L-arginine [31, 49]. The Metropolis Monte Carlo method embedded in Adsorption Locator module in Materials studio software[36, 50-52], provides four step types for a canonical ensemble: conformer, rotation, translation, and re-growth [53]. Figure 7a represents the most stable L-arginine configuration adsorbed on Fe(111) surface in presence of the simulated synthetic reservoir water. Also, Fig. 7a shows the adsorption sites on L-arginine molecule. The adsorption density of L-arginine on the Fe(111) surface in aqueous solution has been presented in Fig. 7b. As can be seen from Figs. 7a and 7b that the L-arginine molecule shows the ability to adsorb on Fe surface. The calculated binding energy of L-arginine and the steel surface reaches $-189 \text{ kcal mol}^{-1}$ using the following equation:

$$E_{\text{binding}} = E_{\text{total}} - (E_{\text{surface}} + E_{\text{inhibitor}}) \tag{5}$$

where E_{total} is the total energy of the surface and inhibitor, E_{surface} is the energy of the Fe (111) surface without the inhibitor, and $E_{\text{inhibitor}}$ is the energy of the inhibitor without the surface.

The descriptors and outputs obtained by the Monte Carlo simulation method are presented in Fig. 7c . These calculated parameters include total energy of the corrosion system. The total energy represent the sum of the energies of the L-arginine molecules, the rigid adsorption energy and the

deformation energy of L-arginine. In this study, the energy of the steel surface is considered as zero. In addition, adsorption energy represents energy released (or required) when the relaxed L-arginine molecules in simulated synthetic reservoir water are adsorbed on the steel substrate. The adsorption energy is defined as the sum of the rigid adsorption energy and the deformation energy for the L-arginine molecules. The rigid adsorption energy reports the energy released (or required) when the unrelaxed L-arginine molecules (i.e., before the geometry optimization step) are adsorbed on the steel surface. The deformation energy reports the energy released when the adsorbed L-arginine molecules are relaxed on the steel surface. Fig. 7c shows also (dE_{ads}/dN_i) , which reports the energy of substrate-adsorbate configurations where one of the L-arginine molecule has been removed. Figure 7d shows the adsorption energy distribution of the L-arginine molecules on steel surface. As can be seen in Fig. 7c, the adsorption energy of L-arginine reaches $(90.8 \text{ kcal mol}^{-1})$ which shows the adsorption power for L-arginine molecules on steel surface.

5. CONCLUSION

The main conclusions of the present study can be summarized as follows:

- The scale and corrosion inhibition studies show that L-arginine may be considered as a multifunction inhibitor.
- The electrochemical measurements (Electrochemical impedance spectroscopy, EIS, potentiodynamic polarization and linear polarization measurements) indicated that, under the used experimental conditions L-arginine gives sufficient inhibition for steel corrosion in synthetic reservoir water.
- The results of EIS show that the value of CPEs tends to decrease and both charge transfer resistance and inhibition efficiency tend to increase as the inhibitor concentration increases.
- Potentiodynamic polarization measurements showed that the L-arginine affects both the cathodic and anodic electrode processes and thus it acts as a mixed-type inhibitor.
- Molecular modeling has become popular in efforts to save time and energy in actual syntheses and test runs while still being able to take factors such as surface temperature, pH, and solution chemistry into consideration.

ACKNOWLEDGMENTS

This research is financially supported by the King Abdul Aziz City for Science and Technology, KACST (Project # AT-32-7) and Taif University (Project# 1-346-4541) in Kingdom of Saudi Arabia. Authors are very grateful for this financial support.

References

1. W. Wittke, *J. Met. Finishing*, 87 (1989) 24.
2. M. Yamada, N. Fukumura, T. Iwanaga, M. Saruwatari, *Corrosion-resistant parts for precision machines prevented from metal contamination*, in, Nippon Fusso Co., Ltd., Japan . 2015, pp. 20pp.

3. G. Xu, Y. Chen, B. Zhao, B. Dong, L. Jing, H. Li, D. Chen, G. Li, *Method for preventing contact corrosion of aluminum alloy and titanium alloy parts*, in, No.601 Institute of Aviation Industry Corporation of China, Peop. Rep. China . 2015, pp. 5pp.
4. Y. Wang, *Improved ferric sulfate with good flocculation effect and corrosion inhibition effect for wastewater treatment*, in, Suzhou Xinxieli Environmental Protection Technology Co., Ltd., Peop. Rep. China . 2015, pp. 4pp.
5. R.X. Sun, P.F. Wang, D.D. Zhao, Z.Z. Sun, C.Q. Li, K.Z. Chen, *Mater. Corros.*, 66 (2015) 383-386.
6. L.S. Zivkovic, J.P. Popic, B.V. Jegdic, Z. Dohcevic-Mitrovic, J.B. Bajat, V.B. Miskovic-Stankovic, *Surf. Coat. Technol.*, 240 (2014) 327-335.
7. J. Zhang, *An environmental friendly corrosion inhibitor for corrosion prevention field of automobile cooling systems*, in, Chery Automobile Co., Ltd., Peop. Rep. China . 2014, pp. 7pp.
8. L.F.G. Williams, *Corros. Sci.*, 13 (1973) 865-868.
9. C. Lemaître, B. Baroux, G. Beranger, *Werkstoffe und Korrosion*, 40 (1989) 229-236.
10. A. Bahadur, *Mater. Trans., JIM*, 34 (1993) 1191-1194.
11. M. Bethencourt, F.J. Botana, J.J. Calvino, M. Marcos, M.A. Rodríguez-Chacón, *Corros. Sci.*, 40 (1998) 1803-1819.
12. A. Aballe, M. Bethencourt, F.J. Botana, M.J. Cano, M. Marcos, *Werks. Korros.*, 52 (2001) 344-350.
13. A.I. Altsybeeva, V.V. Burlov, N.S. Fedorova, S.M. Reshetnikov, *Int. J. Corros. Scale Inhib.*, 2 (2013) 277-286, 210 pp.
14. N.s. Zhang, C.j. Wei, X. Chen, J.x. Han, H.h. Ge, *Corrosion and Protection*, 33 (2012) 419-421.
15. J.B. Sun, G.A. Zhang, W. Liu, M.X. Lu, *Corros. Sci.*, 57 (2012) 131-138.
16. B. Labriti, N. Dkhireche, R. Tourir, M.E. Touhami, M. Sfaira, A. El Hallaoui, B. Hammouti, A. Alami, *Arabian Journal for Science and Engineering*, 37 (2012) 1293-1303.
17. J.I. Bregman, *Corrosion inhibitors*, The Macmillan company, New York-USA, 1963.
18. H.A. Alsaïari, N. Zhang, S. Work, A. Kan, M.B. Tomson, 2012.
19. T. Chen, P. Chen, H. Montgomerie, T. Hagen, H. Ekpeni, *Development of environmentally friendly calcium carbonate scale inhibitor for HTHP squeeze application in the oil and gas field water treatment*, in, 2011.
20. J.I. Bregman, *Ind. Eng. Chem.*, 52 (1960) 63A-64A.
21. K. Khaled, *J. Solid State Electrochem.*, 13 (2009) 1743-1756.
22. K.F. Khaled, *Electrochim. Acta*, 53 (2008) 3484-3492.
23. N.O. Eddy, E.E. Ebenso, *J. Mol. Model.*, 16 (2010) 1291-1306.
24. N.O. Eddy, *Port. Electrochim. Acta*, 27 (2009) 579-589.
25. N.O. Eddy, F.E. Awe, A.A. Siaka, L. Magaji, E.E. Ebenso, *Int. J. Electrochem. Sci.*, 6 (2011) 4316-4328.
26. A. Kalendová, D. Veselý, *Anti Corros. Method M.*, 55 (2008) 175-190.
27. C. Kamal, M.G. Sethuraman, *Ind. Eng. Chem. Res.*, 51 (2012) 10399-10407.
28. C. Kamal, M.G. Sethuraman, *Arab. J. Chem.*, 5 (2012) 155-161.
29. K. Barouni, L. Bazzi, R. Salghi, M. Mihit, B. Hammouti, A. Albourine, S. El Issami, *Mater. Lett.*, 62 (2008) 3325-3327.
30. K.F. Khaled, N.S. Abdelshafi, A. El-Maghraby, A. Aouniti, N. Al-Mobarak, B. Hammouti, *Int. J. Electrochem. Sci.*, 7 (2012) 12706 - 12719.
31. K.F. Khaled, N.S. Abdelshafi, *Int. J. Electrochem. Sci.*, 8 (2013) 1409 - 1421.
32. Zarrouk, B.Hammouti, H. Zarrok, M. Bouachrine, K.F. Khaled, S.S. Al-Deyab, *Int. J. Electrochem. Sci.*, 7 (2011).
33. K.F. Khaled, N.S. Abdel-Shafi, *Int. J. Electrochem. Sci.*, 6 (2011) 4077-4094.
34. K.F. Khaled, A.M. El-Sherik, *Int. J. Electrochem. Sci.*, 8 (2013) 10022 - 10043.
35. K.F. Khaled, A.M. El-Sherik, *Int. J. Electrochem. Sci.*, 8 (2013) 9918 - 9935.
36. Y. Tan, *Corros. Sci.*, 53 (2011) 1145-1155.
37. G. Gece, *Corros. Sci.*, 53 (2011) 3873-3898.

38. H. Ma, S. Chen, L. Niu, S. Zhao, S. Li, D. Li, *J. Appl. Electrochem.*, 32 (2002) 65-72.
39. K.F. Khaled, N.A. Al-Mobarak, *Int. J. Electrochem. Sci.*, 7 (2012) 1045-1059.
40. Zarrouk, B. Hammouti, H. Zarrok, M. Bouachrine, K.F. Khaled, S.S. Al-Deyab, *Int. J. Electrochem. Sci.*, 7 (2012) 89-105.
41. H. Ashassi-Sorkhabi, N. Ghalebsaz-Jeddi, F. Hashemaddeh, H. Jahani, *Electrochim. Acta*, 51 (2006) 3848-3854.
42. R.S. Gonçalves, D.S. Azambuja, A.M. Serpa Lucho, *Corros. Sci.*, 44 (2002) 467-479.
43. L. Beaunier, I. Epelboin, J.C. C. Lestrade, H. Takenouti, *Surf. Technol.*, 4 (1976) 237.
44. K.F. Khaled, S.S. Abdel-Rehim, G.B. Sakr, *Arab. J. Chem.*, 5 (2012) 213-218.
45. K.F. Khaled, *J. Electrochem. Soc.*, 158 (2011) S28-S28.
46. L. Han, S. Song, *Corros. Sci.*, 50 (2008) 1551-1557.
47. E.M. Sherif, S.M. Park, *Electrochim. Acta*, 51 (2006) 1313-1321.
48. K.F. Khaled, N.S. Abdel-Shafi, N.A. Al-Mobarak, *Int. J. Electrochem. Sci.*, 7 (2012) 1027-1044.
49. K.F. Khaled, *J. Chem. Acta*, 1 (2012) 59-65.
50. H. Tamura, *Corros. Sci.*, 50 (2008) 1872-1883.
51. J. Tang, Y. Shao, T. Zhang, G. Meng, F. Wang, *Corros. Sci.*, 53 (2011) 1715-1723.
52. M.T. Gudze, R.E. Melchers, *Corros. Sci.*, 50 (2008) 3296-3307.
53. C. Guedes Soares, Y. Garbatov, A. Zayed, G. Wang, *Corros. Sci.*, 50 (2008) 3095-3106.

© 2016 The Authors. Published by ESG (www.electrochemsci.org). This article is an open access article distributed under the terms and conditions of the Creative Commons Attribution license (<http://creativecommons.org/licenses/by/4.0/>).